PSFC/JA-01-5

Electronic Excitation Temperature Profiles in an Air Microwave Torch

K. Green, M. C. Borrás, P. P. Woskov, G. J. Flores III,
K. Hadidi, and P. Thomas

January 2001

Plasma Science and Fusion Center
Massachusetts Institute of Technology
Cambridge, MA 02139

This work was supported by the U. S. Department of Energy, Office of Science and Technology, Mixed Waste Focus Area.

Submitted for publication to *IEEE Transactions on Plasma Science*

Electronic Excitation Temperature Profiles in an Air Microwave Plasma Torch

K.M. Green, M.C. Borrás, P.P. Woskov, G.J. Flores III, K. Hadidi, P. Thomas

Massachusetts Institute of Technology, Plasma Science and Fusion Center,

167 Albany Street, Cambridge, MA 02139

Abstract — A 0.9 to 1.5 kW, 2.45 GHz atmospheric pressure air microwave plasma torch has been operated efficiently with less than 1 % reflected power. The plasma is sustained in a 28 mm internal diameter fused quartz tube which penetrates perpendicularly through the wide walls of a tapered and shorted WR-284 (72 x 17 mm cross-section) waveguide. A study has been made of the effects of power and airflow on the electronic excitation temperature, T_{exc}. Abel inversion of radial profile chord averaged Fe I emission lines in the 370 to 377 nm range have been used to obtain localized profile measurements of T_{exc} inside the waveguide excitation region. In general, temperature profiles peak on axis with no evidence of a skin effect in the large diameter (10 mm FWHM emission intensity) plasmas. A maximum central T_{exc} of 6550 K ± 350 K is observed at an airflow rate of 28 lpm. When maintaining a constant flow rate of 14 lpm, a 55 % increase in microwave power from 0.9 to 1.4 kW causes a ~100 % increase in plasma volume without any noticeable effect on the central T_{exc} value. At a constant microwave power of 1.4 kW, an increase in total flow rate from 11 to 28 lpm decreases the volume of the plasma by ~25 % and increases the central T_{exc} by ~13 %. The axially peaked temperature profiles are consistent with an electron density of ~ 10^{13} cm^{-3}.

Index terms: electronic excitation temperature, microwave plasma, atmospheric pressure plasma, atomic emission spectroscopy

I. INTRODUCTION

Considerable interest exists in medium to high-power, atmospheric pressure microwave sustained plasmas for environmental and industrial processing as well as monitoring applications. The main advantages of such plasmas are electrodeless operation, high throughput atmospheric processing, efficient microwave to plasma coupling, and availability of inexpensive sources at 0.915 and 2.45 GHz. Low power (< 500 W) atmospheric pressure microwave-induced plasmas (MIPs) have had a long history of use for laboratory spectroscopic analysis instrumentation. Such plasmas can be formed in resonant cavity, waveguide, or surface-effect systems [1]. The plasma gas typically consists of argon, helium, nitrogen, or air [1]-[4]. More recently, there have been studies and applications of higher power (>1 kW) microwave plasmas to increase plasma robustness for laboratory spectroscopic analysis [5, 6], continuous emissions monitoring in the field [7], commercial processing [8], and other applications [9].

Atmospheric microwave plasmas can operate over a wide range of electron plasma density regimes from low density glow-discharge like plasmas [8, 9] to higher density arc-discharge like torch plasmas [5-7]. The work reported here focuses on a microwave plasma torch (MPT) under development for continuous emissions monitoring of smokestack hazardous metals air pollution. The MPT can be a reliable stack mounted technology for real-time atomic emission spectroscopy of trace metals [7]. However, the excitation efficiency in an air plasma for some metals with high electronic excitation energies is not as high as in a plasma without oxygen in the gas matrix [10,11]. Understanding how the electronic excitation temperature may

be increased in an atmospheric air MPT would be of value for reducing the detection limits for some important pollutants such as mercury and arsenic.

Atmospheric pressure microwave plasmas are not as well studied as radio frequency inductively coupled plasma (ICP) systems. Numerous plasma temperature studies have been performed of ICPs. In these studies the temperature is lower in air plasmas, which impedes the excitation of the sample species and, therefore, depresses the characteristic atomic line emission. Gomes et al. [12] report lower temperatures in air ICP plasmas than in argon ICP plasmas, explaining that the polyatomic species in air store energy in their excited levels. Abdallah and Mermet [13] report that a few percent of nitrogen introduced into an argon ICP plasma also reduces the plasma temperature. In the case of a MPT, Hadidi et al. [10] have shown that the addition of oxygen to a nitrogen plasma decreases the rotational and electronic excitation temperatures. Since the presence of molecular species is inherent to an air MPT for application as a stack pollution monitor, the objective of the experiments reported here is to examine the effect of other parameters such as microwave power level and volume of gas flow on the electronic excitation temperature.

II. Experimental Setup

The experimental setup used is shown in Figure 1. The microwave generator is an ASTeX Model S-1500i 1.5 kW, 2.45 GHz magnetron source. The output of the magnetron is connected by WR-284 waveguide to a circulator, which in turn is connected to a triple stub impedance matching tuner and a water-cooled reflected power dump. A Teflon window seals the output of the triple stub tuner to keep the circulator and magnetron clean of dust from the

plasma end of the waveguide. Microwave detectors at the magnetron input to the circulator and at the circulator output to the dump continuously monitor forward and reflected power. During the present experiments, the forward microwave power is varied over the range of 0.9 kW to 1.4 kW. The reflected power can be adjusted with the triple stub tuner to less than 1 % of the forward power. Even with all the tuning stubs completely withdrawn reflected power is typically less than 10%.

The plasma is sustained by the microwaves in a tapered and shorted waveguide attached to the windowed end of the triple stub tuner. The cross-section of the waveguide at the tapered plasma end is 72 x 17 mm. The plasma gas flow is confined inside a quartz tube with a 32 mm outside diameter and a 2 mm thick wall. This quartz tube penetrates through the center of the wide waveguide walls one-quarter (30.6 mm) waveguide wavelength back from the short where the E-field is peaked before the plasma is started. There is no resonator structure. Once the plasma is started the microwaves are beamed directly into the absorbing plasma without obstruction. The plasma is started with a small tungsten Hertz spark loop on the tip of an alumina rod, which is briefly inserted into the quartz tube in the waveguide.

Tangentially injected swirl airflow into the quartz tube upstream of the waveguide keeps the plasma off the inside walls of the quartz, confining the plasma to the center of the tube. An axial airflow transports the sample to be atomized and excited by the plasma for spectroscopic study. The swirl and the axial airflows typically each make up half of the total gas flow through the plasma. A branch in the axial airflow line connects to a sample feed source. The sample feed source consists of a pneumatic nebulizer and a spray chamber. The nebulizer aerosolizes a weak acid solution containing the element to be studied and ejects the mist into a spray chamber

at a rate of ~1 ml/min each for the liquid and drive gas feed rates. The spray chamber limits water loading by filtering large droplets (over 99 % of the original solution) into a waste container [14]. The branch line is heated to volatilize the liquid droplets as they are transported to the plasma.

The plasma emission light is viewed through a large aperture in the waveguide short. The aperture is beyond the cut off for transmission of 2.45 GHz radiation with a cross-section of 32 x 12.7 mm and a depth of 30 mm. A pair of quartz lenses image and magnify, by a factor of two, the plasma light onto a plane where a fiber optic cable is used to scan the plasma diameter. The fiber optic is a UV quartz cable with a core diameter of 0.8 mm and a numerical aperture of 0.22. Data collection occurs for up to sixty-six chords that are evenly spaced in one-millimeter increments.

The fiber optic is connected to an Instruments S.A. Model THR-640, 0.64 m spectrometer which has a 2400 groove/mm grating, an adjustable slit, and a Princeton Instruments Model IRY-512W intensified 512-element detector array. For the present experiments with atomic iron emission, this spectrometer is tuned to cover the 370 – 377 nm spectral range with a spectral resolution of about 0.05 nm.

The sample feed uses an Alpha Aesar calibrated solution having a concentration of 10,000 μg/ml of iron dissolved in a 5% solution of nitric acid. To obtain accurate emission levels when the aerosol iron sample is injected into the plasma, deionized water is first injected to obtain a blank water background spectrum. Subtracting the water background from the iron

spectrum removes the influence of the water loading on the plasma light intensity. The influence of the nitric acid on the plasma is assumed negligible, and all remaining signal light is assumed due only to the influence of the iron in the plasma. Figure 2 shows a representative iron spectrum obtained in the present setup.

III. THEORY

A. Abel Inversion

The Abel inversion allows for the transformation of line-integrated data to localized values [15]. In the case of the microwave plasma torch, the Abel inversion technique permits transforming the line-integrated plasma light intensity, *I(y)*, into the localized radial emissivity, *ε(r)*. Figure 3 illustrates the analytical geometry and defines some of the parameters. The line-integrated intensity and the radial emissivity are respectively given by [16]

$$I(y) = 2\int_{y}^{R} \frac{\varepsilon(r)}{\sqrt{r^2 - y^2}} r dr \tag{1}$$

$$\varepsilon(r) = -\frac{1}{\pi}\int_{r}^{R} \frac{\frac{dI(y)}{dy}}{\sqrt{y^2 - r^2}} dy \tag{2}$$

where R is the maximum plasma radius. The units for the line integrated intensity and for the radial emissivity are $Wm^{-3}sr^{-1}$ and $Wm^{-4}sr^{-1}$, respectively.

The Abel inversion technique requires a symmetric intensity function as well as the necessity for the intensity to fall to zero at the plasma edge [17]. To ensure that these specifications are met, a subtracted Gaussian is fit to the intensity profile data of each iron line. This curve has the form

$$I(y) = Ae^{-by^2} - Ae^{-bR^2} \tag{3}$$

where A and b are fitting parameters unique to each intensity profile. Each iron line is inverted using Equation 2 to obtain the derived radially localized emissivity

$$\varepsilon(r) = \frac{1}{\sqrt{\pi}} Ab^{\frac{1}{2}} e^{-br^2} erf\left(\left[b\left(R^2 - r^2\right)\right]^{\frac{1}{2}}\right) \tag{4}$$

where r is the radial parameter.

B. Determination of T_{exc}

The excitation temperature, T_{exc}, is determined by fitting a thermal distribution to the appropriately weighted intensities of a set of atomic transitions for a specific atomic species in the plasma [18]. In the case of the MPT experiments, the atomic species used is iron. The localized intensities, I_{ij}, of neutral atomic iron, Fe I, transitions are the quantities obtained by the

Abel inversion of the measured chord averaged intensities in the MPT system. The iron lines of interest fall in the range between 368 nm to 377 nm. To yield $T_{exc,}$ the appropriate statistics and oscillator strengths are used to scale the intensities. Each observed Fe I wavelength has an associated energy level, E_j, a statistical weight, g_i, and oscillator strength, f_{ij}, as given in Table I [19]. The calculation of T_{exc} at a particular radius entails plotting $\log(I_{ij}\lambda^3 / g_i f_{ij})$ versus E_j [18]. The slope of a straight line fit to these points relates to the electronic excitation temperature by

$$T_{exc} = -\frac{0.625}{m} \tag{5}$$

where T_{exc} is in K, and m is the slope of the line [15]. The deviation from a straight line determines the error in T_{exc}.

Performing this calculation at each radial point provides the T_{exc} profile in the plasma. Since the light emission levels decline rapidly near $r = 10\ mm$, the error in T_{exc} becomes quite large beyond this range. Therefore, the T_{exc} profile measurements extend only to this radius.

A key assumption in this analysis of T_{exc} is that neutral atomic iron and the electrons are each in thermal equilibrium. If the plasma is shown to be in or near local thermodynamic equilibrium (LTE), then this assumption is valid. The condition of LTE specifies that all temperatures in the plasma are equal except the blackbody radiation temperature [15]. LTE requires that the collisional processes dominate the radiative processes in the plasma [17].

C. Determining Proximity to LTE

Griem [20] has established a criterion for the determination of a plasma's proximity to LTE. This formulation places a lower limit on the electron density. The Griem criterion states

$$n_e \geq 9\times10^{11}\left(\frac{\Delta E}{E_H}\right)^3\sqrt{\frac{T_e}{E_H}} \qquad (6)$$

where n_e is the electron density in cm^{-3}, ΔE is the energy level difference between the ground state and the first ionization state, E_H is the ionization potential for hydrogen (13.6 eV), and T_e is the electron temperature. Equation 6 is valid only for optically thin plasmas.

Evaluation of the Griem criterion necessitates knowledge of the electron temperature, T_e and density, n_e. Neither of these parameters could be directly measured in the present experiment, but a number of past results in atmospheric microwave plasmas can be used to estimate these values. Potts *et al.* [8] and Brandenburg *et al.* [9] have measured T_e of 1.1 and 0.67 eV, respectively, and have measured a n_e of ~ 7 x 10^{10} cm^{-3} in spatially extended ball lightning like microwave plasmas. In a more dense microwave torch plasma, Ogura et al [6] have measured a n_e of ~ 3 x 10^{13} cm^{-3} at 1 kW microwave power level in atmospheric pressure nitrogen. Timofeev [21] has also developed an electron density expression based on experimental data from an atmospheric pressure spherically symmetric microwave air discharge. The electron density is given by

$$n_e = \begin{cases} 5.91\times10^{15} e^{-\frac{14.42}{T-1.74}} & (T > 1.74) \\ 0 & (T < 1.74) \end{cases} \quad (7)$$

where n_e is in cm^{-3}, and T is the temperature at LTE measured in 10^3 K. Anticipating our temperature measurements below, Equation 7 results in n_e of ~ 2 x 10^{14} cm^{-3}.

Evaluating Equation 6 for an electron temperature of approximately 1 eV and for a ΔE corresponding to the ionization potential for the N_2 molecule (15.6 eV) results in an electron density threshold of ~3 x 10^{11} cm^{-3} for LTE. This value is well below the electron densities for an atmospheric microwave torch plasma and near the measured values for the more tenuous ball lightning like microwave plasmas. Therefore, based on the Griem criteria the assumption of LTE is believed to be valid for the MPT T_{exc} analysis presented here. Further support for the validity of this assumption can be found in Borrás [22] where measurements of the rotational temperature in the present MPT system in nitrogen are presented and are approximately the same as the T_{exc} measurements presented below.

IV. Experimental Results

A. As a Function of Microwave Power

For the experiments at different forward microwave power levels, the total airflow rate is held constant at 14 lpm. The data are collected at three power levels, 900 W, 1150 W, and

1400 W. Figure 4 shows one of the chord averaged emission intensity profiles for the 373.5 nm Fe I transition at 1400 kW. The points represent experimental measurements, and the line is a best fit of Equation 3. The agreement between the subtracted Gaussian profile and the experiment is good. This profile is typical for other iron transitions and other power levels. Though all the measured profiles have a similar shape to that of Figure 4, the light emission intensity diameter and level increase with microwave power over the studied power range.

Figure 5 depicts the Abel inverted and normalized light emission profiles for a representative Fe I transition. Quite noticeable is the increase in plasma size. The Abel inverted light emission intensity profiles are also well represented by Gaussian profiles peaked on axis, as expected. No evidence of profile flattening or going over to a hollow profile with increasing microwave power is observed to suggest a finite microwave absorption depth less than the maximum plasma radius.

As the forward microwave power is increased by 55 % from 900 W to 1400 W, the plasma diameter full width at half maximum (FWHM) increases from 4.5 to 6.5 mm. This growth corresponds to an increase in the plasma cross-sectional area and volume inside the waveguide by over 100 %. This observation is consistent with other RF driven atmospheric plasmas. Abdallah and Mermet [23] report an inflation in their inductively-coupled argon plasma with an increase in power.

Using the localized emission intensities of 12 or more Fe I transitions such as the one shown in Figure 5, a T_{exc} temperature fit is obtained as described in Section II.B. A

representative temperature fit is shown in Figure 6 for the axial temperature at 1400 W. Temperature fits such as this are done at each radial position across the scanned plasma radius. The emission light levels where strong enough on the weak Fe lines only out to a plasma radius of 10 mm to do a temperature fit. The resulting T_{exc} temperature profiles are shown in Figure 7. The temperature profiles are almost flat out to the largest measurable plasma radius of 10 mm with a maximum of 5800 K ± 200 K on axis. At the 10 mm radius this temperature is still 80% of its value on axis, where the plasma emission intensity is less than a few percent of its on axis value. Increasing the microwave power has no effect within the error bars of the measurements on the temperature of the plasma. This observation is consistent with other atmospheric microwave plasma work. Timofeev has reported that increasing the microwave power by two orders of magnitude produces only a minor effect on the plasma temperature of an atmospheric pressure microwave plasma discharge and flat profiles within a spherical discharge [21]. The additional microwave power contributes to expanding the plasma volume rather than heating the plasma to a higher temperature.

B. As a Function of Airflow

For the experiments at different airflow rates, the forward microwave power is held constant at 1400 W. Four total airflow rates, 11 lpm, 14 lpm, 23 lpm, and 28 lpm, are examined. For the 14 lpm case, the axial airflow constitutes 8 lpm while the swirl airflow makes up 6 lpm of the total flow. For all of the other airflow rates, the axial and swirl airflows constitute equal portions of the total.

Figure 8 displays the results of this study for a representative Fe I transition. The localized light emission profiles have been normalized to the same value on axis. The plasma diameter decreases slightly as the total airflow rate increases. For a total airflow rate increase of 11 lpm to 28 lpm the plasma radius at FWHM decreases from 7.0 to 6.0 mm corresponding to a cross-sectional area or plasma volume decrease inside the waveguide of 27 %. This result suggests an improved confinement of the plasma by increasing the total airflow rate.

The electronic excitation temperature is again obtained by utilizing the localized plasma light emission intensities of 12 or more Fe I transitions like the one shown in Figure 8. The resulting T_{exc} profiles for the various airflows are plotted in Figure 9. The temperature profiles are again almost flat, but now an increase in temperature is observed as the airflow increases. The axial temperature increases 13 % from 5800 K ± 200 K to 6550 K ± 350 K over the range of airflow studied. For the highest airflow at 28 lpm the temperature data is possible only out to an 8 mm radius because of the decrease in the plasma light emission diameter. The temperature profile at the highest flow also looks much flatter.

The observed temperature increase with airflow is contrary to expectations. Increasing the flow velocity through the plasma is expected to cool the plasma and reduce temperatures. Ogura *et al*. [6] report the lowest electronic excitation values with the highest carrier gas flow rate. This decrease is attributed to an increased plasma loading of particulates and a reduced plasma residence time. In the present MPT case increasing the axial flow rate does not correspondingly increase the feed rate and apparently a decreased residence time does not reduce the plasma temperature within the range of flow velocities of the present experiment.

V. DISCUSSION

A. Interpretation of T_{exc} Profiles

The lack of dependence of T_{exc} on the microwave power can be understood in terms of the high collisionality of atmospheric pressure plasmas. The atmospheric microwave plasma is weakly ionized even for the highest electron density torch plasmas. The dominant electron collisions are with neutrals. As given in Timofeev [21] this collision frequency can be estimated by $\nu(T) = n(T) v_e(T) \sigma$, where $n(T) = n_o T_o / T$ is the neutrals density, n_o is the Loschmidt number (2.69 x 10^{19} cm^{-3}), T_o is room temperature, $v_e(T) = \sqrt{3kT/m_e}$, and σ is the cross-section for electron-neutral collisions which is assumed to be 10^{-15} cm^2. For the measured MPT temperature of 5800 K the electron-neutral collision frequency is thus estimated as 7 x 10^{10} s^{-1}. During one 2.45 GHz microwave cycle, an electron experiences more than 25 collisions with a mean free path between collisions of about 7 μm. The microwave electric field has insufficient time to accelerate the electrons to a high energy before inelastic collisions with neutrals cause the electrons to lose energy.

The internal energy states in an air plasma matrix limit the electron temperature through the high collision rate. However, all the microwave energy is absorbed as the forward power is increased. The measurements show that at a constant airflow rate this added energy goes to increasing the plasma volume rather than increasing the temperature. This fact is not a detriment for a MPT air metals pollution monitor. Estimates show that the sample species in the axial flow diffuses away from the center of the plasma as the gas flows through the waveguide [24]. The

expansion of the plasma diameter at high microwave power ensures an enlarged region in which the species may experience excitation. If the plasma is optically thin, which is the case for most metals of interest, the extra light emission can be collected to increase detection limits. This technique is in fact utilized when the MPT is viewed axially rather than radially to increase the light collection path length in the plasma to obtain lower detection limits [7].

Unfortunately, not all atomic emissions are optically thin in an atmospheric plasma and therefore a larger plasma does not help. In the important case of mercury the strongest transitions terminate on the ground state. Consequently, the unexcited atoms cause self-absorption [11]. In this case the excitation efficiency must be increased to the lower detection limits, which requires more electrons with energies above the 4.9 eV excitation energy for mercury.

The measurements show that higher plasma temperatures are possible with higher airflow rates that cause the plasma to become more constricted. In Figure 6, the plasma volume decreases by ~27% as the gas flow rate increases from 11 lpm to 28 lpm. The peak temperature on axis correspondingly increases by ~13% as shown in Figure 9. This improved plasma confinement may, in part, be attributed to a high swirl flow rate in the 28 lpm total gas flow rate regime. The microwave energy absorbed does not change and thus with the smaller plasma volume the temperature rises. Therefore, for improving MPT performance for monitoring applications of some metals such as mercury, this result suggests that engineering smaller constricted microwave plasmas of high power could produce higher temperature for more efficient atomic excitation.

B. Skin Depth

The plasma cross-section size that can be driven efficiently by microwaves will be determined by what the absorption depth or skin depth is in the plasma. The results presented here demonstrate that the skin depth for the present MPT must be of the order of the plasma radius. If it were much more there would be large reflected power. If it were less the emissivity profiles in these figures would display a flattening or hollowing near the center of the plasma as observed in ICP plasmas with skin depths less than the plasma radius [25]. Therefore, the skin depth for the MPT must be about 0.5 cm for single pass absorption to be efficient.

Lieberman and Lichtenberg [26] describe the collisional skin depth, δ, by

$$\delta = \frac{\sqrt{2}c}{\omega_{pe}}\left(\frac{\nu}{\omega}\right)^{\frac{1}{2}} \tag{8}$$

where c is the speed of light in a vacuum, $\omega_{pe} = \sqrt{e^2 n_e / \varepsilon_o m_e}$ is the electron plasma frequency in radians s^{-1}, ν is the momentum collision frequency in Hz, and ω is the microwave frequency in radians s^{-1}. Equation 8 is valid only if ω_{pe}, $\nu >> \omega$, which is true for the present MPT experiments.

Evaluation of Equation 8 requires knowledge of the electron density, which was not measure. However, this equation can be rearranged to solve for the electron density using the

observed plasma radius as the skin depth and the collision frequency derived above. The resulting electron density is ~ 10^{13} cm^{-3}, which is consistent with the MPT measurements of Ogura et al [6]. This result suggests that the formalism of Equation 8 can be used to understand MPT performance. The observed increase in plasma temperature and continued efficient microwave absorption in a smaller plasma size agree with this model. Because of the dependence of the collision frequency on temperature, the skin depth will decrease as the temperature increases allowing total absorption by smaller plasmas. The electron density will probably also increase with temperature to help this scaling. Thus efficient higher temperature microwave plasmas should be possible for application to mercury monitoring.

Large MPT plasma dimensions are also possible, which can be of value to many processing applications that require electrodeless plasma operation. Conventional wisdom states that scaling RF driven ICP torches to higher power and larger dimensions requires going to lower frequencies. This reasoning is based on the frequency scaling of the skin depth. However, the atmospheric MPT plasma cross-section compares favorably with lower frequency RF driven ICPs at comparable powers. In addition, the MPT has a much higher coupling efficiency of electromagnetic energy to the plasma. Therefore, the MPT may be a superior technology for applications where electrodeless plasma operation is important.

VI. Conclusions

Electronic excitation temperature profile measurements in an atmospheric pressure air microwave plasma torch over a power range of 900 to 1400 W show that power has little effect

on temperature with all other parameters such as airflow rate held constant. Over this power range, T_{exc} remains constant at 5800 ± 200 K on axis with an almost flat temperature profile. The temperature decreases by less than 20% out to a radius of 10 mm where the plasma light emission has decreased by more 95% of the on axis intensity. Increasing power only causes the plasma diameter to become larger, leading to an increase in the plasma volume by about 100% over the studied power range.

The electronic excitation temperature does increase when the plasma column is confined to a smaller diameter by increased axial and swirl airflow. Increasing the total airflow from 11 to 28 lpm reduces the plasma volume by about 25 % and increases the electronic excitation temperature by about 13 % to 6550 ± 350 K. The continued efficient absorption of all the microwave power with smaller plasma cross-section is consistent with a collisional skin depth model when temperature also increases. The efficient atmospheric microwave plasma torch should find useful applications where electrodeless and high throughput operations are important.

ACKNOWLEDGEMENT

The research presented in this text was sponsored by the Mixed Waste Focus Area, Office of Science and Technology, Environmental Management, U. S. Department of Energy.

REFERENCES

[1] A. T. Zander and G. M. Hieftje, "Microwave-supported discharges", *Applied Spectroscopy* vol. 35, no.4, pp. 357 –371, 1981.

[2] K. Fallgatter, V. Svoboda, and J. D. Winefordner, "Physical and analytical aspects of a microwave excited plasma", *Applied Spectroscopy*, vol. 25, no. 3, pp. 347 –352, 1971.

[3] K. A. Forbes, E. E. Reszke, P. C. Uden, and R. M. Barnes, "Comparison of microwave-induced plasma sources", *J. of Analytical Atomic Spectrometry*, vol. 6, pp. 57 –71, February 1991.

[4] K. C. Ng and W .L. Shen, "Solution nebulization into low-power argon microwave-induced plasma for atomic emission spectrometry: study of synthetic ocean water", *Anal. Chem*, vol. 58, pp. 2084 –2087, 1986.

[5] Y. Okamoto, "Annular-shaped microwave-induced nitrogen plasma at atmospheric pressure for emission spectrometry of solutions", *Analytical Sciences*, vol. 7, pp. 283 –288, April 1991.

[6] K. Ogura, H.Yamada, Y Sato, and Y. Okamoto, Excitation temperature in high-power nitrogen microwave-induced plasma at atmospheric pressure", *Applied Spectroscopy*, vol. 51, no. 10 pp. 1496 –1499, 1997.

[7] P. P. Woskov, K. Hadidi, P. Thomas, K. Green, and G. Flores, "Accurate and sensitive metals emissions monitoring with an atmospheric microwave-plasma having an real-time span calibration", *Waste Management*, vol. 20, pp. 395-403, 2000.

[8] H. Potts and J. Hugill, "Studies of high-pressure, partially ionized plasma generated by 2.45 GHz, microwaves", *Plasma Sources Sci. Technol., vol. 9, pp. 18-24, 2000.*

[9] J. E. Brandenburg and J. F. Kline, "Experimental Investigation of Large-Volume PIA Plasmas at Atmospheric Pressure", *IEEE Trans. on Plasma Sci.*, vol. 26, no. 2, pp. 145-149, 1998.

[10] K. Hadidi, P. P. Woskov, G. J. Flores, K. Green, and P. Thomas, "Effect of oxygen concentration on the detection of mercury in an atmospheric microwave discharge", *Jpn. J. Appl. Phys.*, vol. 38, pp. 4595-4600, 1999.

[11] K. Hadidi, P. P. Woskov, K. Green, and P. Thomas, "Observation of self absorption of mercury I and cadmium I emission in an atmospheric microwave sustained plasma", *J. Anal. At. Spectrom.*, vol. 15, pp. 601-605, 2000.

[12] A. M. Gomes, J. Bacri, J. P. Sarrette, and J. Salon, "Measurement of heavy particle temperature in a radiofrequency air discharge at atmospheric pressure from the numerical

simulation of the NOγ system" *Journal of Analytical Atomic Spectrometry*, vol. 7 pp. 1103 – 1109, October 1992.

[13] M. H. Abdallah and J. M. Mermet, "The behavior of nitrogen excited in an inductively coupled argon plasma", *J. Quant. Spectrosc. Radiat. Transfer*, vol. 19, pp. 83 –91, 1978.

[14] G. J. Flores, "Establishing a calibration for a microwave plasma continuous emissions monitor", Master 's Thesis, Massachusetts Institute of Technology, Nuclear Engineering Department, 1998.

[15] P. W. J. M. Boumans, editor, *Chemical Analysis*, vol. 90, John Wiley & Sons, Inc., New York, Chapters 10-11, 1987.

[16] K. Miyamoto, *Plasma Physics for Nuclear Fusion*, The MIT Press, Cambridge, Massachusetts, revised edition, 1989.

[17] I.H.Hutchinson, Principles of Plasma Diagnostics, Cambridge University Press, Cambridge, 1994.

[18] J. P. Matousek, B. J. Orr, and M. Selby, "Microwave-induced plasmas: Implementation and application", *Prog. analyt. atom. Spectrosc.*, vol. 7, pp. 275 –314, 1984.

[19] J. F. Alder, R. M. Bombelk, and G. F. Kirkbright, "Electronic excitation and ionization temperature measurements in a high frequency inductively coupled argon plasma source and the influence of water vapor on plasma parameters", *Spectrochimica Acta B*, vol. 35, pp.163 –175, 1980.

[20] H. R. Griem, *Plasma Spectroscopy*, McGraw-Hill Book Company, New York, 1964.

[21] A. V. Timofeev, "Theory of microwave discharges at atmospheric pressures", *Plasma Physics Reports*, vol. 23, no. 72, pp. 158 –164, 1997.

[22] M. C. Borrás, K. Hadidi, P. Woskov, K. M. Green, G. J. Flores, and P. Thomas, "An experiment for radial temperature profile measurements in a microwave induced plasma at atmospheric pressure", IEEE Conference Record-Abstracts, p. 169, 1998 IEEE International Conference on Plasma Science, Raleigh, NC, June 1-4, 1998.

[23] M. H. Abdallah, and J. M. Mermet, "Comparison of temperature measurements in ICP and MIP with Ar and He as plasma gas", *Spectrochimica Acta B* , vol. 37, no. 5, pp. 391 –397, 1982.

[24] B. R. Pollack, "Establishing isokinetic flow for a plasma torch exhaust gas diagnostic for a plasma hearth furnace", Master 's Thesis, Massachusetts Institute of Technology, Nuclear Engineering Department and Mechanical Engineering Department, 1996.

[25] M. I. Boulos, “The inductively coupled RF (radio frequency) plasma”, *Pure & Appl. Chem.*, vol. 57, no. 9, pp. 1321-1352, 1985.

[26] M. A. Lieberman and A. J. Lichtenberg, *Principles of Plasma Discharges and Materials Processing*, John Wiley & Sons, Inc., New York, 1994.

Table I. Fe I Emission Lines Used for T_{exc} Determination [19]

Wavelength, λ (nm)	E_j (cm^{-1})	$10^{20}\lambda/gf$ (m^3)
368.222	55754	2.6202
368.411	49135	9.5279
370.108	51192	5.1878
370.446	48703	18.8875
371.993	26875	13.8549
372.438	45221	25.8918
372.762	34547	17.1512
373.239	44512	16.4422
373.486	33695	2.5517
373.713	27167	19.3916
374.826	27560	53.8876
374.948	34040	3.5638
375.823	34329	5.3082
376.379	34547	8.258
376.554	52655	1.5757
376.719	34692	11.6964

Figure Captions

Figure 1. Experimental setup of the microwave plasma torch for atomic emission profile measurements.

Figure 2. Typical atomic iron (Fe I) spectrum observed in the MPT.

Figure 3. Geometry for Abel inversion.

Figure 4. Radial profile of the chord averaged plasma emission intensity at the 373.5 nm Fe I transition. Points are experimental measurements and the line is a fit of Eq. 3.

Figure 5. Normalized light emission at constant flow rate with varying power for a representative Fe I transition.

Figure 6. Temperature fit to localized iron transition emission intensities on axis.

Figure 7. Electronic excitation temperature at constant flow for different microwave forward power levels.

Figure 8. Normalized light emission at constant power with varying flow rate for a representative Fe I transition.

Figure 9. Electronic excitation temperature at constant microwave power for different total gas flow rates.

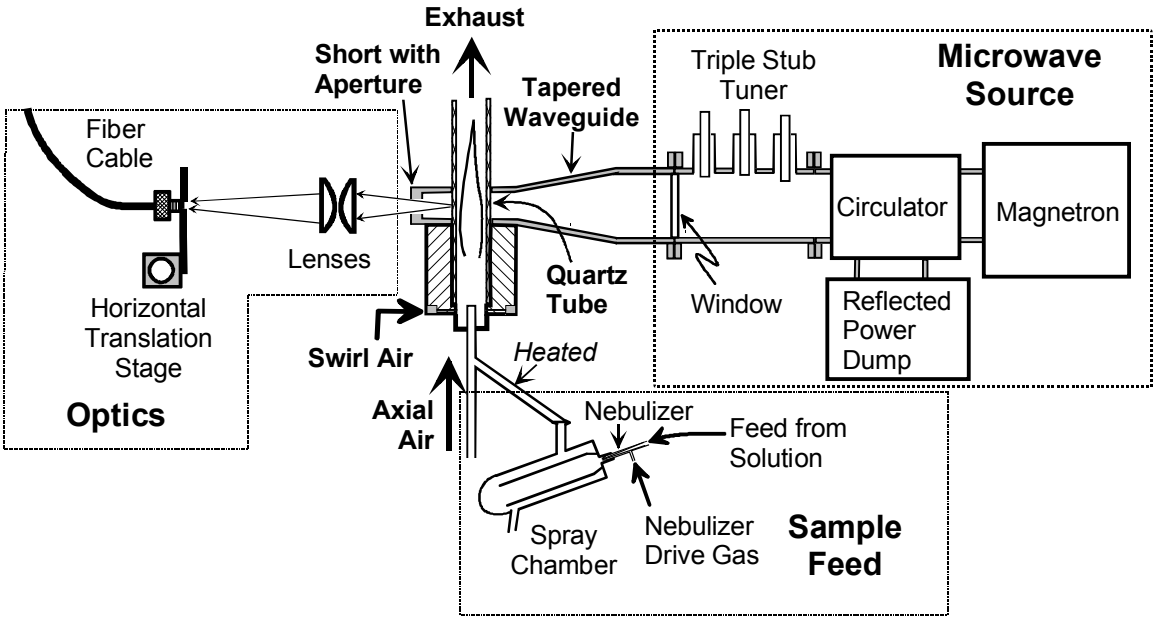
Exhaust
Short with Aperture
Tapered Waveguide
Triple Stub Tuner
Microwave Source
Fiber Cable
Circulator
Magnetron
Lenses
Quartz Tube
Window
Reflected Power Dump
Horizontal Translation Stage
Swirl Air
Heated
Optics
Axial Air
Nebulizer
Feed from Solution
Spray Chamber
Nebulizer Drive Gas
Sample Feed

Figure 1.

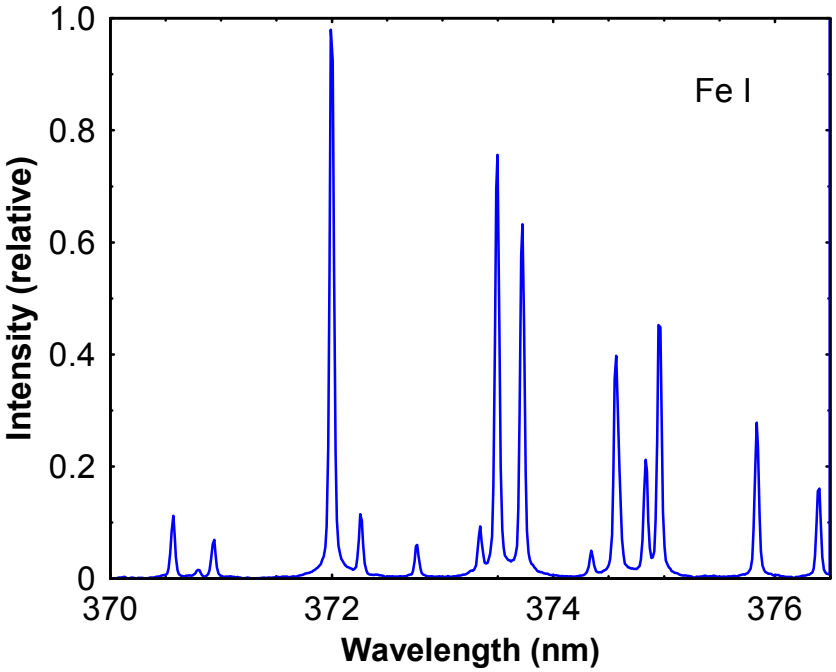
Fe I
Intensity (relative)
Wavelength (nm)
1.0
0.8
0.6
0.4
0.2
0
370
372
374
376

Figure 2.

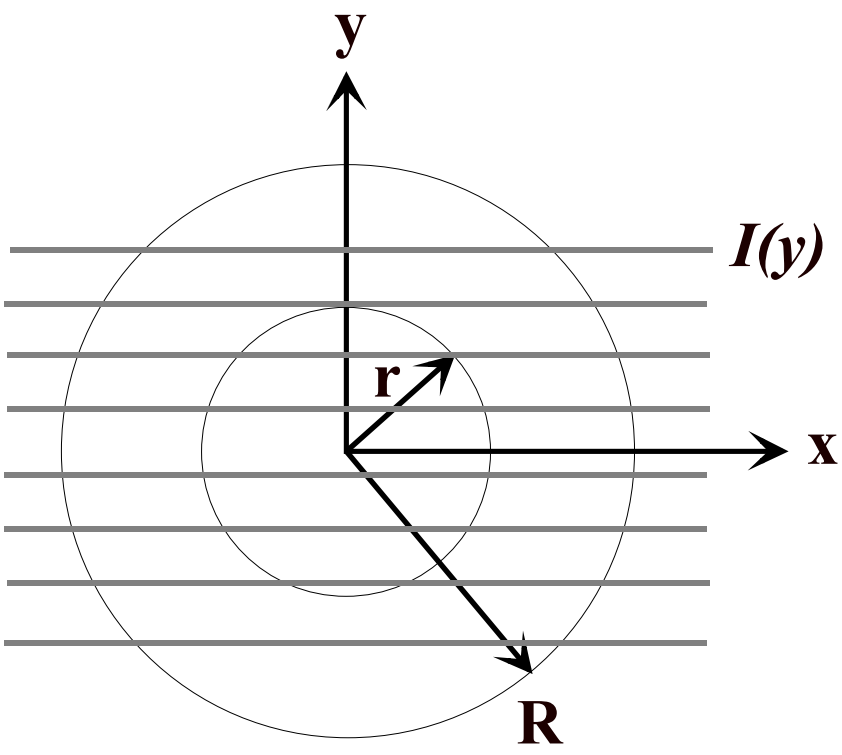

Figure 3.

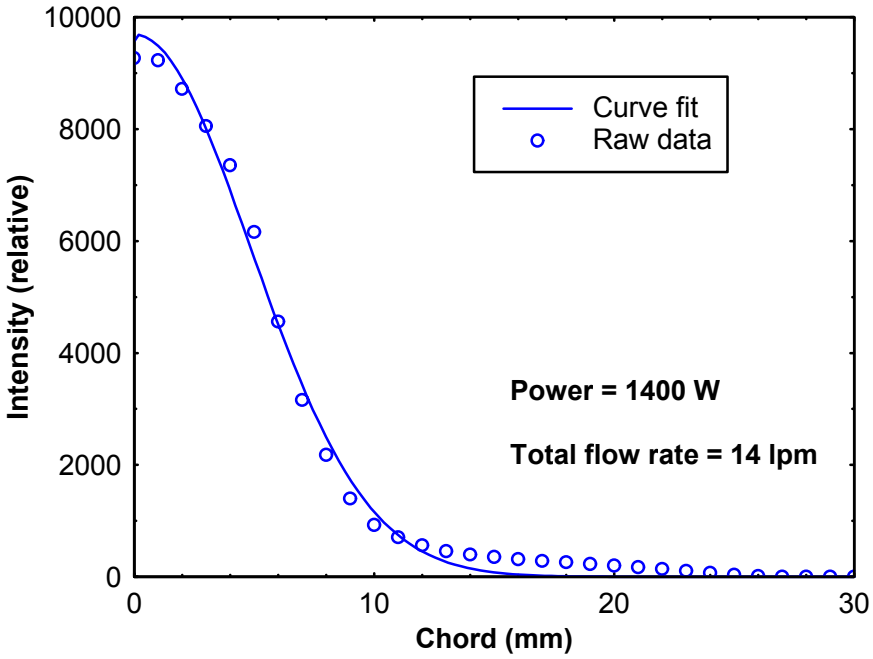
10000
8000
6000
4000
2000
0
Intensity (relative)
0
10
20
30
Chord (mm)
Curve fit
Raw data
Power = 1400 W
Total flow rate = 14 lpm

Figure 4.

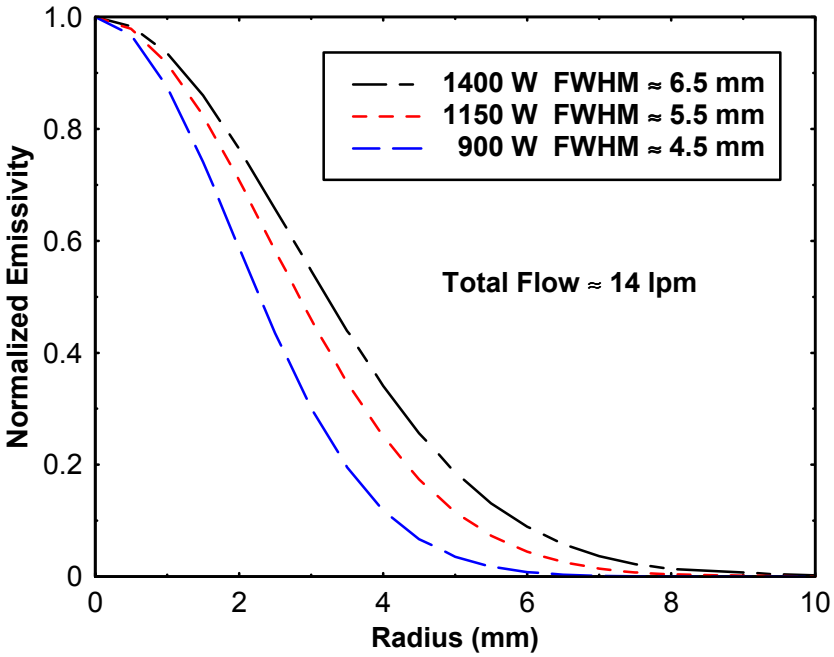
1400 W FWHM ≈ 6.5 mm
1150 W FWHM ≈ 5.5 mm
900 W FWHM ≈ 4.5 mm
Total Flow ≈ 14 lpm
Normalized Emissivity
Radius (mm)
0
0.2
0.4
0.6
0.8
1.0
0
2
4
6
8
10

Figure 5.

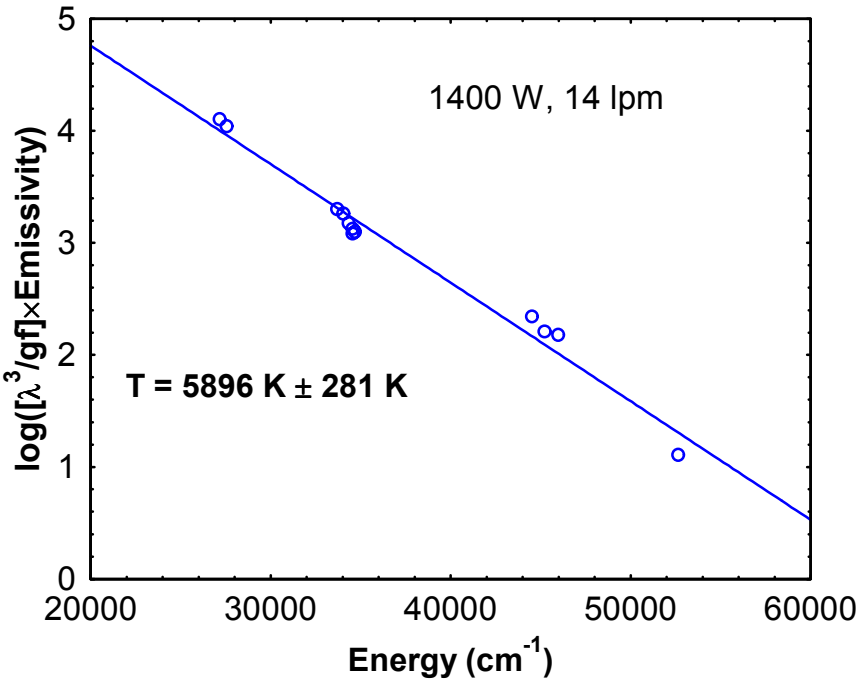
1400 W, 14 lpm
T = 5896 K ± 281 K
log([Iλ^3/gf]×Emissivity)
Energy (cm^{-1})
0
1
2
3
4
5
20000
30000
40000
50000
60000

Figure 6.

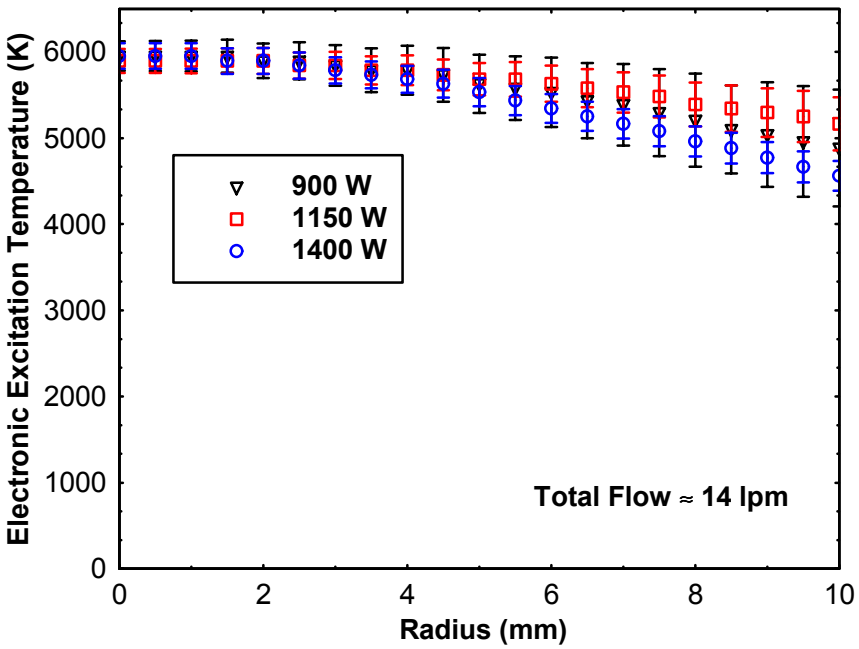
Electronic Excitation Temperature (K)
6000
5000
4000
3000
2000
1000
0
0
2
4
6
8
10
Radius (mm)
900 W
1150 W
1400 W
Total Flow ≈ 14 lpm

Figure 7.

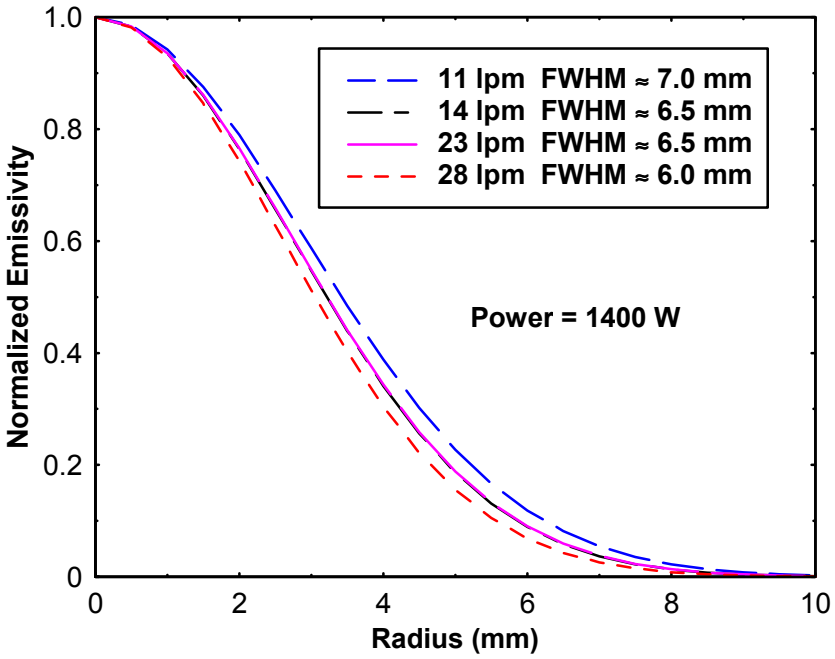
1.0
0.8
0.6
0.4
0.2
0
Normalized Emissivity
0
2
4
6
8
10
Radius (mm)
11 lpm FWHM ≈ 7.0 mm
14 lpm FWHM ≈ 6.5 mm
23 lpm FWHM ≈ 6.5 mm
28 lpm FWHM ≈ 6.0 mm
Power = 1400 W

Figure 8

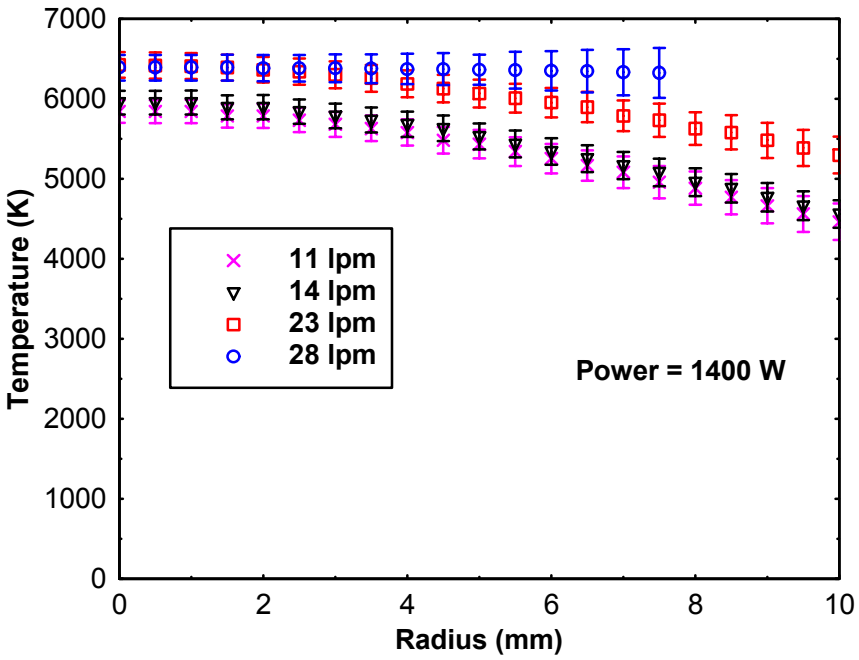
7000
6000
5000
4000
3000
2000
1000
0
Temperature (K)
0
2
4
6
8
10
Radius (mm)
11 lpm
14 lpm
23 lpm
28 lpm
Power = 1400 W

Figure 9